2020

Differential calretinin interneuron morphology in the primary visual cortex versus the lateral prefrontal cortex in the monkey and mouse

BOSTON UNIVERSITY

SCHOOL OF MEDICINE

Thesis

DIFFERENTIAL CALRETININ INTERNEURON MORPHOLOGY IN THE PRIMARY VISUAL CORTEX VERSUS THE LATERAL PREFRONTAL CORTEX IN THE MONKEY AND MOUSE

by

JUNWOO PARK

B.A., Boston University, 2017

Submitted in partial fulfillment of the

requirements for the degree of

Master of Science

2020

Approved by

First Reader

Jennifer I. Luebke, Ph.D.
Waterhouse Professor and Chair of Anatomy & Neurobiology

Second Reader

Maria Medalla, Ph.D.
Assistant Professor of Anatomy & Neurobiology

ACKNOWLEDGMENTS

I am greatly indebted to my family for supporting my academic career without question. Nothing would have been possible without your kind sacrifice, mom and dad.

I am also sending great thanks to my advisors, Jennifer Luebke and Maria Medalla for academic guidance and helping me getting mature as a scientific researcher. I can tell myself became so positively changed from me before joining the lab. A year working with you passed like a sudden. But I have a hunch that I will never forget this period ever in my life.

I would like to express my gratitude to my lab mates. Rakin, Chelsey, Alexa, Wayne, Emma, Dhruba, Ana, Diego, and Yuxin. Thank you for teaching me the lab techniques I did not know and providing me useful criticisms. It was a pleasure working with you all.

Finally, I am grateful to my roommates, Woosik and Himchan, who went through all my ugliness but kept understanding. Thank you for standing beside me.

DIFFERENTIAL CALRETININ INTERNEURON MORPHOLOGY IN THE PRIMARY VISUAL CORTEX VERSUS THE LATERAL PREFRONTAL CORTEX IN THE MONKEY AND MOUSE

JUNWOO PARK

ABSTRACT

In the mammalian neocortex, GABAergic interneurons play a variety of roles in higher-order brain functions as key components of brain circuits. Many studies have revealed properties of pyramidal neurons, but the functions of interneurons are relatively poorly understood. Focusing on inter-species differences, previous work in our lab (Gilman et al, 2017) revealed pyramidal neuron differences in monkey and mouse primary visual (V1) and frontal (FC) cortices. Here, we designed a comparative study in a similar context to reveal knowledge of Calretinin (CR)-expressing interneurons in monkey and mouse V1 and area FA of the mouse, prefrontal cortical area 46, and V1 of the monkey. Monkey and mouse brain tissues were immuno-stained, scanned with a confocal microscope and 3D reconstructed using NeuroLucida 360. Semi-automated analyses revealed that mouse CR interneurons on both brain regions were larger and showed more dendritic branching. Cell type sorting following the previous classification method by Cauli et al (2014) showed distinctive cell type distribution Monkey V1. CR interneurons in V1 regions in both species showed features that differentiate them from FC interneurons, including more node counts than those in FC. Also, a sudden increase in average V1 dendritic diameter after its 75% length progression was shown between species. These findings have provided gap-filling

knowledge about CR+ interneuron species-specific differences in V1 and PFC, which gives a foundation for inter-species data comparison.

TABLE OF CONTENTS

LIST OF TABLES

LIST OF FIGURES

LIST OF ABBREVIATIONS

ANOVA	Analysis of Variance
CLSM	Confocal Laser Scanning Microscopy
CR	Calretinin
dmPFC	Dorsomedial Prefrontal Cortex
EPSP	Excitatory postsynaptic potential
GABA	Gamma Aminobutyric Acid
IHC	Immunohistochemistry
LPFC	Lateral Prefrontal Cortex
MGE	Medial Ganglionic Eminence
MKY	Monkey
MOM	Mouse on Mouse
MRI	Magnetic Resonance Imaging
MSE	Mouse
NIH	National Institute of Health
NL360	NeuroLucida 360

PFC	Prefrontal Cortex
PLoS	Public Library of Science
PV	Parvalbumin
SA	Surface Area
V1	primary visual cortex
V4	visual area V4
Vgat	Vesicular GABA Transporter
WT	Wild Type

INTRODUCTION

Mammalian Neocortex: General Principles

As prefix ‘Neo’ means ‘New’ in Latin, the emergence of neocortex occurred later compared to other parts of the brain. There is a view that the prototype of the neocortex has emerged from reptiles, during the transition between the Devonian and Permian periods. However, the 6 layered composition of the mammalian neocortex is thought to have emerged between the Triassic and Jurassic period (Rakic P, 2010). The complexity of the mammalian neocortex has further developed, which varied between species and in timing. Such differences in neocortical development caused variations between species. Now the organization of mammalian neocortex shows both primitive similarities and distinct features which are exclusive to species.

As an example of interspecies similarity, the embryonic neocortical development of monkey, mouse, and humans is remarkably similar. The very first closeness can be found in the neuron laminar placement in the neocortex. Newborn neurons of all species are not generated in the neocortex. Instead, they are generated in progenitor areas, which are medial ganglionic eminence (MGE), caudal ganglionic eminence, and preoptic area (Gotz et al, 2005). Specifically, newborn excitatory neurons, which make up the majority of the neurons in the cortex, migrate radially from the ventricular zone and distributed vertically. For the majority of inhibitory neurons, they commonly migrate from MGE. Fully grown pyramidal neurons and interneurons form horizontal sheets, which are stacked on top of

each other. As a result, stacked sheets of neurons form a 6-layer composition of the neocortex.

Each layer of the neocortex is different with regard to the neuron population and functions. Pyramidal neurons are abundant in layers 2 and 3, which send vertical projections to other layers, which form an output connection between layers, other cortical regions, and even to another hemisphere (Quiquempoix et al, 2018). Layer 4 serves as the main thalamic input layer of the neocortex, which contains dense distributed spiny stellate cells (Hubel and Wiesel, 1962). Other than layer-specific specialization, myeloarchitecture of layers varies by the functionally different brain regions. For instance, layer 4 is well developed in the primary visual cortex (V1) as a consequence of major thalamic input (Arkhipov et al, 2018). As a result, the primary visual cortex shows the distinct band looking lamination, which could be universally found among V1 cortices of mammalian species.

Although neocortical organization between species show a similar pattern, there are some major differences between species as well. A noticeable difference is the difference in cortical surface area. Mammalian embryos go through similar stages of development in early stages, but major differences emerge at the later stage of development, which can be seen in the difference of cortical folding (Sun and Hevner, 2014). As a result, differences in the brain between species emerge. One of the major differences is the amount of surface area expansion. There are various hypotheses suggested for this phenomenon. The social intelligence hypothesis, suggests that the surface area of the brain increased as the social complexity increases (Lindenfors, 2005). For example, there are observational results that

social complexity and neocortex sizes are positively correlated in primate groups (Barton, 1996). This leads to the possible inference that there are different social demands between each animal species, which is reflected in morphological variances of brain shapes and neocortical surface areas. Likewise, there could be other interspecies differences found in the neocortex, specifically within the neuron population, and during their development.

Interneurons: Origin and Functions

As previously described, mammalian embryos follow universal developmental steps in their early stage. Newly born progenitor cells migrate radially and end up in layer to function as fully grown cells. There are several fates that progenitor cells grow to. One of them is a pyramidal neuron. Pyramidal neurons, which are named after their morphology, project to other neurons in different layers and the opposite hemisphere (Qi and Feldmeyer, 2015, Koestinger et al, 2017). These connections form cortical networks, which are the key structures that regulate and perform brain functions. Although pyramidal neurons play a significant role in building a foundation of brain structure, they are not the only building blocks of circuits in the neocortex. Interneurons, which are the other types of neurons, show different placements in the cortex. Interneurons are inhibitory neurons that creating local circuits between pyramidal neurons by making connections between their axons, dendrites, and somas (Huang et al, 2007).

The presence of interneurons has been known since the early 20th century, which occurred a few decades after the discovery of pyramidal neurons by Ramon y Cajal. In 1929, Rafael Lorente, who was the youngest student of Cajal, depicted the various

morphology of various types of neurons, some of which resemble a known morphology of interneurons. He also depicted accurately about their placement, located within a single layer and connecting pyramidal neurons (Fairen, 2007).

What do interneurons do in the neocortex, among pyramidal neurons? Although they only comprise 20% of total populations of cortical cells, interneurons regulate signal and information flows between neurons by connecting between pyramidal neurons (Hu et al, 2017). For instance, activities of excitatory neurons are necessary for voluntary controls by signaling either stop or go command of ongoing movement (Ghosh et al, 2014). However, if the intensity of excitatory and inhibitory signals are altered intended actions cannot be implemented, which is commonly seen in Huntington's disease phenotypes (Chen et al, 2013). In order to initiate the right amount of excitatory activation, we need a mechanism to suppress the right amount of excitatory output. This is the role that inhibitory interneurons play. In the mammalian neocortex, the activity of an excitatory neurons is regulated by cortical inhibitory interneurons, in a process called local inhibition (Meganathan et al, 2017).

There are numerous types of interneurons, which are usually classified by their different shape, neurotransmitter content, and mechanism of action. Such properties of interneurons are used to classify them; morphological, electrophysiological, and neurochemical properties. Interneurons are named after distinct calcium-binding proteins expressed in them, which are part of their neurochemical properties (DeFelipe et al, 2013). Interneurons with different names have unique regulatory effects on neurons and specific

neocortical positions in the brain. In this thesis, I will focus on two major subtypes of interneurons, calretinin interneurons, and parvalbumin interneurons.

Calretinin Interneurons

Calretinin (CR), which is also known as 29kDa calbindin is one of the proteins expressed in cortical interneurons. It was named after the structural similarity with calbindin D28k (Rogers 1987). While major interneuron populations are generated from medial ganglionic eminence (MGE), only a minor portion of CR positive (+) interneurons are generated from MGE (Fogarty et al, 2007). The major portion of CR+ interneuron populations is generated from caudal ganglionic eminence and distributed to layer 2 and 3 (Cauli et al, 2014). The preoptic area was suggested as another source of CR interneurons, but the generated population was thought to be not relevant enough to discuss (Gelman et al, 2009). However, a recent study showed the density of CR+ neurons fluctuates abruptly during the embryonic stage of brain development (Bogus-Nowakowska, 2018), which could indicate migration of newly generated CR+ neurons from the preoptic area.

Fully developed CR interneurons co-express numerous neuropeptides, which are strong evidence of their multiple roles in neurophysiology. CR cells co-express other markers, but some of the co-expressed markers vary by species. 30% mouse CR interneurons co-express VIP, while the rate boosts up to 70-90% in rat CR interneurons. 30-40% of mouse CR cells express SOM, however, such populations are absent in rats and humans (Cauli et al, 2014).

CR cells have Bipolar or Double Bouquet cell morphology and their dendrites tend to be positioned vertically towards layer 1 and layer 5/6 (Barinka and Druga, 2010). However, there are multipolar and horizontally positioned interneurons that do not follow that dendritic position. Mouse CR cells have shown bipolar and thin morphology, and CR cells in rat consists of 17% of the total GABAergic population, in mouse, it was 18% (Xu et al 2010).

Roles of CR interneurons

The role of CR neurons derives from their structure. The ef-hand domain is a common structure found on calcium-binding proteins. Specifically, the ef-hand domain in CR allows both fast and slow binding with calcium ions, which affects pre- and postsynaptic calcium signals (Faas et al, 2007, Camp and Wijesinghe, 2009). As a modulatory mechanism, CR can also bind to copper ions, which acts as an antagonist of calcium binding to CR (Groves and Palczewska, 2001). There is a view that the population of CR affects motor ability. In several mice studies using various CR expression models, loss of CR in mossy cells of the dentate gyrus and granule cells of the cerebellar cortex induced mildly impaired motor coordination (Barinka and Druga, 2010).

Meanwhile, there is a view that CR plays a neuroprotective role in the neocortex, which mainly focuses on the functions of intracellular calcium. Intracellular calcium works as a key component for neuronal plasticity (Fröhlich, 2016) and other cellular functions of neurons. An excessive amount of intracellular calcium causes improper dendritic growth,

which ultimately leads to cell death (Mattson and Kater, 1987). The ones who claim CR plays a neuroprotective role suggest calcium-binding ability of CR. However, such topics remains highly controversial (Schwaller 2014).

CR+ interneurons receive multiple inputs from various sources, and they emit outputs to surrounding cells and structures. Main neurochemical inputs from brain areas include acetylcholine (basal forebrain), serotonin (raphe), norepinephrine (locus coeruleus), dopamine (ventral tegmental area) (reference). Inputs from surrounding cells include GABA (fast-spiking PV cells, Martinotti cells) and glutamate (pyramidal cells). CR+ cells also send inputs to each other, which is mainly GABAergic, but using enkephalin for volume transmission (reference). CR+ cell output is similar to the within-population input, which forms GABAergic synapse to fast-spiking PV basket cells and Martinotti cells (Cauli et al, 2014). Interestingly, CR+ interneurons in hippocampal areas are known to specifically target other interneurons, which are mainly GABAergic (Klausberger and Somogyi, 2008). Electrophysiologically, CR interneurons exhibit high input resistance (Kawaguchi and Kubota, 1996). which enables them to be depolarized by relatively small excitatory synaptic inputs.

Parvalbumin Interneurons

As with CR, parvalbumin (PV) is also a calcium-binding protein expressed in cells, which also uses ef-hand domain calcium-binding sites. PV plays a role in the muscle contraction-relaxation cycle by modulating calcium level in sarcoplasm (Celio and Heizmann, 1982). In the neocortex, PV is often found among GABAergic inhibitory

neurons, which are specifically classified as PV positive interneurons. PV+ interneuron populations are further divided into basket, translaminar and chandelier cells by their morphological types (Xu et al 2010, Lim et al, 2018). Chandelier cells target the axon initial segment, while basket cells mainly synapse on dendrites and soma (Kawaguchi and Kubota, 1997). Most of these neurons exhibit electrophysiologically fast-spiking properties, which are characterized by action potentials with short durations and little to no adaptation during depolarization steps (Descalzo et al, 2005).

Unlike CR+ interneurons, PV+ interneurons are mainly generated from MGE (Lim et al, 2018), and distributed to their laminar locations across layers 2-6. Among those layers, PV+ cells are most prominent in layers 5 and 6 (Tremblay et al, 2016). PV+ interneurons often have long dendrites across layers, which serves as a site for multiple synapses, including its soma (Hu et al, 2014). For example, in hippocampal CA1 and CA3 regions, PV interneurons receive dense synaptic connections, which are mostly excitatory (Gulyas et al, 1999). Among PV+ basket cell populations, functions of the cells vary by their timing of birth. The output of early-born PV cells strengthens during rule consolidations, while late-born PV cells strengthen during new rule encoding (Caroni 2015).

Roles of PV Interneurons

PV interneurons are known for their fast signaling mechanisms, but what is their role in brain circuits? In the hippocampus, PV interneurons are involved in feed-forward

inhibition mechanisms (Hu et al, 2014). The key point of this involvement is in their firing timing, which is early in the process before connected pyramidal neurons fire. Such feedforward inhibition mechanisms with PV interneurons have important roles in signal processing. It either narrows down the action potential initiation via excitatory postsynaptic potential (EPSP) summation (Pouille and Scanziani, 2001) or expands the dynamic range of afferent input of neuronal population (Pouille 2009). Then how do these functions apply in living organisms on a scale of daily activity? Recent investigations on living animals revealed that PV interneurons play an important role in network oscillation, which is critical in cognitive abilities (Bartos et al, 2007).

The fast-spiking characteristic of PV cells is hypothesized to be the key mechanism of various high order brain functions, including working memory ability (Ferguson and Gao, 2018, Kim et al, 2016). Major neuropsychiatric and neurological diseases, including schizophrenia, depression, epilepsy, and Alzheimer's disease have been associated with abnormal PV interneuron activity (Marin, 2012). Specifically, failure of gamma oscillation was observed in schizophrenia patients, which is mainly due to the deficit of PV+ interneurons for increasing extracellular GABA level (Gonzalez-Burgos et al, 2015). In general, deficiency of the PV interneuron population causes changes to appropriate behavior, which is often found in the prefrontal cortex (PFC) of psychiatric disease patients (Ferguson and Gao, 2018). Moreover, a recent study with mouse model suggested pediatric brain injury may cause PV interneuron loss and greater loss on PV expression (Nichols et al, 2018).

The Social deficit is a common symptom of many psychiatric disorders. A recent study discovered a significant increase of PV+ interneuron activity in the mouse dorsomedial prefrontal cortex (dmPFC) after introducing novel animals with the same age and sex, which represents social interaction. Also, further analysis with optogenetic alteration on dmPFC PV+ cells induced social behavior within 20 seconds after stimulation (Bicks et al, 2020). The role of PV+ interneurons in social behavior is further demonstrated with another study in which researchers found inhibition on the pathway between ventral hippocampus and medial PFC caused impairment on social memory expression that was reversed by stimulating PV+ interneurons in mPFC (Sun et al, 2020). From these results, we can conclude that medial PFC in mouse is an essential area for social behavior, and PV+ interneuron is a key compartment for its function.

Comparative Study between Mouse and Monkey

Due to ethical and practical limitations, scientists were not able to freely utilize human tissue for biological studies. Instead, various animal models have been employed to study the role of interneurons in brain circuits. However, there are interspecies differences that cannot be neglected during interpreting data between studies using different animal models, such as mice and monkeys. Therefore, we designed this comparative study to clarify the differences between these species.

One of the models we used is the mouse model. The mouse model has been widely used for human psychiatric disease research (Dawson et al, 2018). The mouse model is effective due to its gene similarity between human (99%) and their small size contributes

to large study design and cost-effectiveness (Vandamme, 2014). However, whether the mouse is a useful subject or not has been a controversial issue between scientists. There were some arguments saying mouse is the insufficient animal model for human diseases (Seok et al, 2013), but recent studies argue for the sufficiency of the model and set up standards to increase the translational impact of animal studies (Justice and Dhillon, 2016).

On the other hand, the monkey model, which is the other animal model we used, is not as commonly studied as the mouse model. The monkey model has unique strengths compared to mouse models. Monkeys are closer to humans than mice are in the evolutionary distance, and their usefulness in cognitive studies is incomparable to that of mouse models (Phillips et al, 2015).

These two animal brain models share similarities and differences. There is a neocortical size difference (Fig 1B). Rhesus monkey brain is much larger than the mouse brain (Fig 1A), and the size of pyramidal neurons in mice differs in size compared to the pyramidal neurons in monkeys (Gilman et al, 2017). Also, mouse and monkey cortices differ in their area specialization. In this study, we focused on two distinct brain regions, a primary sensory area, the primary visual cortex (V1) and a higher-order multimodal association area, the prefrontal cortex (PFC).

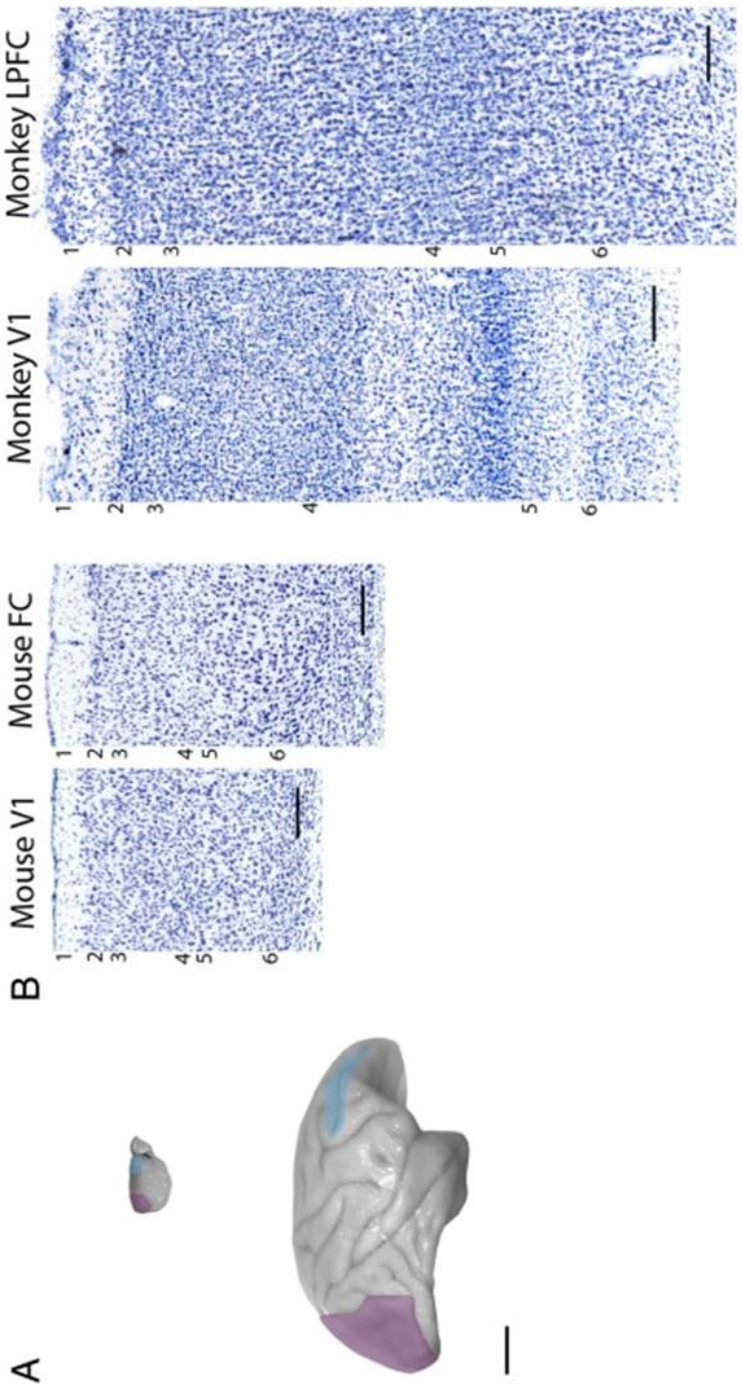

Figure 1. Visual representation of mouse and monkey primary visual and frontal cortices A, 3D model of mouse (up) and monkey (bottom) brain model. Purple highlighted regions are primary visual cortices. Light-blue highlighted regions are frontal cortex in mouse, and lateral prefrontal cortex in monkey. Scale bar size is 1cm B, Nissl-stained coronal section of regions of interest. Scale bar size is 200µm. Figure images and descriptions are imported form Gilman et al, 2017.

Prefrontal Cortex

The prefrontal cortex is more developed in primates, including humans than in rodents. The main function of PFC is executive functions, which incorporates information integration from multiple sensory modalities, attention maintenance, working memory, and language ability (Teffer and Semendeferi, 2012). In other words, PFC is the core region of what we consider as "human" behaviors. Specifically, the lateral region of the prefrontal cortex (LPFC) is believed to be most developed in humans, which does the temporal organization of reasoning, behavior, and speech (Fuster 2001).

The presence of PFC in monkeys is first suggested by Brodmann, which is based on a finding that the granular frontal area is absent or poorly developed in non-primate animals. Another group in recent years tried to evaluate the prefrontal cortex by evaluating magnetic resonance imaging (MRI) scans from multiple primate species (Schoenemann et al, 2005). They concluded humans have significantly larger white matter volume but no difference in gray matter volume, which indicates elaboration of neuronal connection via axon may play a role in complex human cognitive functions. The cognitive abilities of monkeys, although less complex, closely resemble those of humans (Hara et al, 2012). There are numerous cognitive studies done with monkey models, which is difficult to replicate with other animal models.

What about rodents? Since mice and rats are commonly employed animal models in neuroscience studies, there has been a debate on whether rodents are a suitable model for prefrontal cortex studies or not. In fact, the presence of the rodent prefrontal cortex has

been controversial in the field (Uylings et al, 2003). The opposing views against rodent studies are based on the lack of homologs. Rodents and humans diverged from a common ancestor around 96 million years ago (Nei and Glazko, 2002) and have 99% gene similarity. A rodent PFC follows a 6-layered organization just like primates, but the degree of "granularity" differs. Rodent PFC is characterized as agranular or dysgranular, which shows poorly developed layer 4, while primate PFC shows both agranular/dysgranular and granular formations (Uylings et al, 2003, Seamans et al, 2008). Function-wise, primate PFC serves as a center of working memory (Konecky et al, 2017). Likewise, rodents also exhibit working-memory-like behavior by delayed-response tasks (Dudchenko, 2004).

In this study, we studied the premotor region as an analogous region for PFC in the rodent brain, following the approach of previous comparative study (Gilman et al, 2017).

Primary Visual Cortex

V1 is a cortical area that processes visual sensory information. V1 gains inputs from the left and right eye, which is combined to generate a three-dimensional (3D) representation of the surrounding world. A mouse is a widely-used animal model to study V1, but there are several species-wise variances that must be covered before experimental conclusions. First, mice have different anatomical positions of two eyes. Unlike frontal position, which primates have, mouse has lateral positioning of their eyes. Coverage of frontal view drops to 50% on each eye, compared to 135% on primate and humans. Therefore, a visual representation of a mouse is different from humans and monkeys, which

makes ipsilateral LGN axon projection to matching the hemisphere down to 4% (Priebe and McGee, 2014). A famous visual neuron structure, ocular dominance column is also not observed on a mouse.

The monkey V1 has a more similar organization to human V1 compared to mouse V1. Monkeys have frontal eye positions, and ocular dominance columns are present. Groups of researchers validated monkey visual area V4 cortex works similarly with human V4, which elucidated the homology of visual mechanisms between two species (Connor, 2000).

Purpose of this Study

In neuroscientific research, mice and monkeys have both been used as research models, each with unique strengths and weaknesses. Researchers tend to choose the model that fits best for their research interests. However, comparing results between two studies with different models may cause misinterpretation. Previous comparative studies have confirmed differences of pyramidal neurons in PFC and V1 between mouse and monkey subjects (REF). Here we assessed differences in CR and PV interneurons in V1 and PFC between monkey and mouse.

CR+ interneurons are becoming recognized as playing a role in modulating neural circuits and serving as an important regulator of higher-order brain functions (ref). The number of studies using either monkey or mouse CR+ interneurons is increasing. With this study, we aim to present comparative data between mouse and monkey CR+ interneuron, specifically regarding their morphological attributes.

METHODS

Experimental Subjects

Brain tissues from 3 adult wild type (WT, age 8M?) mice and 3 adult Rhesus monkeys (Age= 20, 19, 17.3, 2 females and 1 male) were used in this study. Frontal cortex (FC) area M2 following Allen brain atlas and V1 tissue blocks were taken from WT mice, and LPFC area 46 and V1 tissue blocks were collected from monkeys. WT mice were housed and kept in a 12h light/dark cycle before individual brain harvest at Boston University School of Medicine. All monkeys were part of the larger project in brain and cognition study as a control group subject.

The Boston University School of Medicine is fully approved by the Association of Laboratory Animal Care with animal research and maintenance conducted in strict adherence to animal care guidelines from the National Institute of Health (NIH) *Guide for the Care and Use of Laboratory Animals* and the *U.S. Public Health Service Policy on Humane Care and Use of Laboratory Animals.*

Preparation of Brain Slices and Immunohistochemistry

Mice were deeply anesthetized with sodium pentobarbital (10mg/ml), and perfused by transcardial perfusion with 4% paraformaldehyde. Brain slices were cut at 100μm with the vibratome (Leica VT1000s). Brain slices were processed for immunohistochemistry (IHC) of Parvalbumin (green), Calretinin (Red), and Vgat (far red) as follows. First, tissues were incubated in 65-70C 10mM tri-sodium citrate buffer (pH 8.5) for 20 minutes for

antigen retrieval. Tissue was pre-blocked in 5% BSA in 0.01 PBS (pH 7.4, 4C) with 0.2% Triton-X and Mouse-On-Mouse (MOM) blocking kit (Vector). Then, sections were incubated in the primary antibodies, Rabbit anti-Calretinin (Swant, 1:2000), Mouse anti-Parvalbumin (Swant, 1:1000), guinea pig anti-Vgat (Synaptic Systems, 1:400), for 48 hours (4C). After rinsing, tissue was incubated in donkey secondary antibodies conjugated to Alexa fluorescent probes, donkey anti-rabbit 647; anti-mouse 546; and anti-guinea pig 488, for 24 hours (at 4C). Tissues went through low wattage (150W) microwave for two times (10 min) during all primary and secondary antibody incubations. The final wash was done with 0.1PB (pH 7.4, 4C).

Monkeys were first sedated with ketamine hydrochloride (10mg/ml) and deeply anesthetized with sodium pentobarbital with respect to animal weight (15mg/kg). Monkeys were perfused with ice-cold Krebs-Heinselt buffer (Sigma-Aldrich). The dura was quickly cut to expose the brain during perfusion. A block of tissues ($10mm^3$) were taken from LPFC and V1. Tissues were cut into 300μm slice using a vibratome while submerged in ice-cold oxygenated ringer solutions (concentrations, in mM, 26 $NaHCO_3$, 124 NaCl, 2 KCl, 3 KH_2PO_4, 10 Glucose, 1.3 $MgCl_2$; pH = 7.4, chemicals from Sigma), equilibrated in room temperature for at least 1 hour, and then immersion fixed in 4% paraformaldehyde for 48 hours. Slices were re-sliced to 100μm using a vibratome and then processed for IHC as above, using Rabbit anti CR (Swant, 1:2000), Goat Anti PV (Swant, 1:2000), guinea pig anti Vgat (Synaptic systems, 1:400) primary antibodies. The rest of the step followed the same procedure of mouse IHC.

All sections were mounted, counterstained and coverslipped with Dapi-prolong gold mounting medium. Mouse prefrontal cortex (PFC), defined as mouse frontal association area (FA) (Uylings et al, 2003, Fig 2A, B) versus monkey lateral prefrontal cortex (LPFC), and mouse V1 (Fig 2C, D) versus monkey V1 were the main regions of interest compared.

Confocal Image Acquisition

In order to visualize immunohistochemically labeled calretinin positive (CR+) interneurons, high-resolution Confocal Laser Scanning Microscopy (CLSM) was used. Leica TCS SPE scanned 3D image stacks of somas and dendrites of targeted interneurons using a 40x 1.3 numerical aperture and oil immersion objective, at a resolution of 0.0896x0.0896x0.3μm voxel size. Three channels using 3 distinct excitation wavelengths [546nm (PV), 647nm (CR), and 488nm (Vgat)], were scanned and collected sequentially and merged later. CR+ neurons with complete somata were identified in L2-3 and dendritic arbors were followed and imaged using multiple tile scans which were montaged to trace whole-cell projections.

NeuroLucida Reconstruction

CR+ interneuron in mice and monkeys were identified and reconstructed with NeuroLucida 360 (NL360) version 2019.1.1. All somata were detected by soma estimation which program calculates and dendrites were reconstructed with user-guided tracing, “Direct kernels” mode. All reconstructions went through manual interventions to minimize nonspecific process tracing. All cells used in this study fit into the previously measured

depths and extent of L2-3 in other studies, with somata located within 250-500 µm deep from the pia for monkey V1, 300-700 µm deep for monkey LPFC, and 200-400 µm deep in the mouse V1 and FC (Gilman et al 2016, Medalla and Barbas 2010, Van De werd et al 2010).

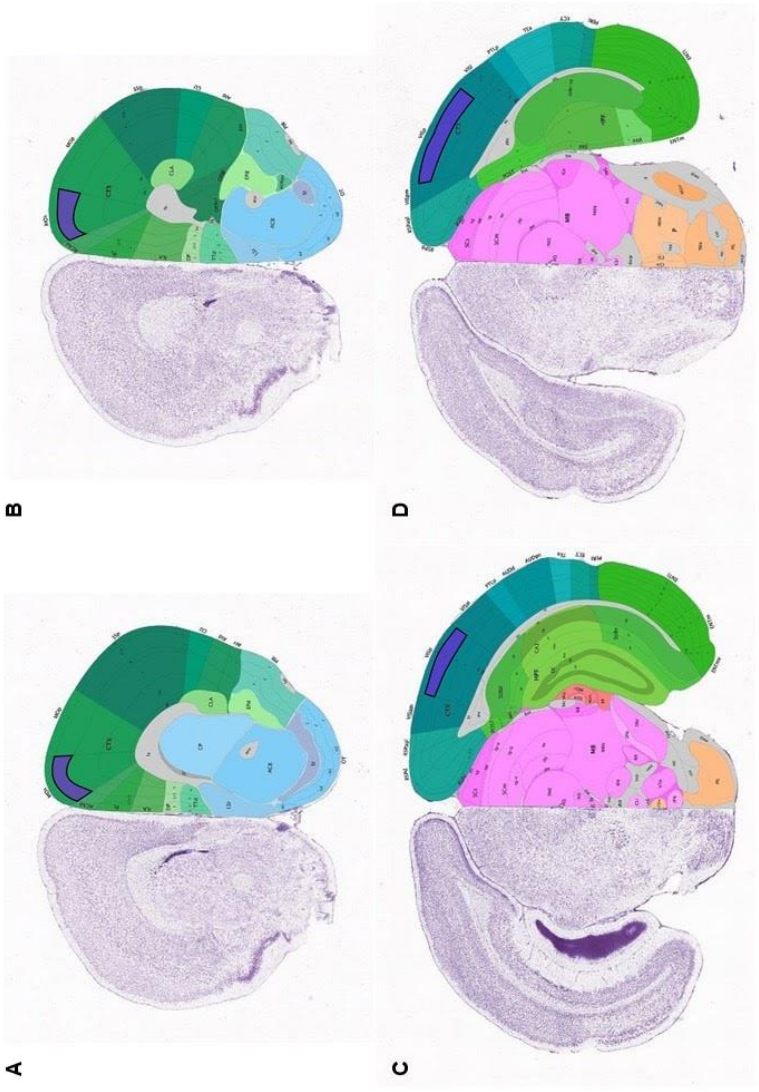

Figure 2. Regions of interest in mouse brain. A, purple highlighted region indicates rostral end of the mouse premotor area, secondary motor cortex layer 2/3. B, caudal end of mouse premotor area layer 2/3. C, purple highlighted region is the rostral end of mouse V1 layer 2/3, D, caudal end of mouse V1 layer 2/3

NeuroLucida Data Analysis

Soma to pia distance and cell types of each reconstructed cell were manually measured by line measure tool in NL360. Cell type determination followed the previous work of Cauli et al, 2014. Bipolar (Fig 3A), single tufted (Fig 3B), bitufted (Fig 3C), modified (Fig 3E) and multipolar (Fig 3F) were used as classification types. Tripolar (Fig 3D) was not used due to its ambiguity. The data from 3D reconstructed CR+ interneurons were obtained via NL360 explorer. Total length and number of nodes in dendrites were obtained by individual total analysis. Surface area (SA) and volume of somata were acquired by a 3D contour summary of the cell body. The calculation formula for cell body data was; SA per cylinder = Perimeter of the profile * Distance to the next profile and Volume = Area of the profile * Distance to the next profile (Fig 4B). Specifically, for 3D cell body SA analysis, formula "surface = [(perimeter Contour 1 + perimeter Contour 2 + ... + perimeter Contour n)/n] * thickness" was used. Sholl analysis with 10μm rings originating from the centroid of soma was performed (Fig 4A) based on previous work (Sholl et al, 1953) contained multiple measurements; Interaction, intersecting length, mean surface area, and the average diameter of dendrites.

Statistical Analysis

Exported data files from NL360 explorer were converted to Microsoft Excel file. Standard deviations and standard errors of means were calculated for the graph generation for this study. Graphpad Prism 8.3.0 was used to perform a one-way analysis of variance (ANOVA) analysis, Tukey, and Bonferroni post hoc analysis.

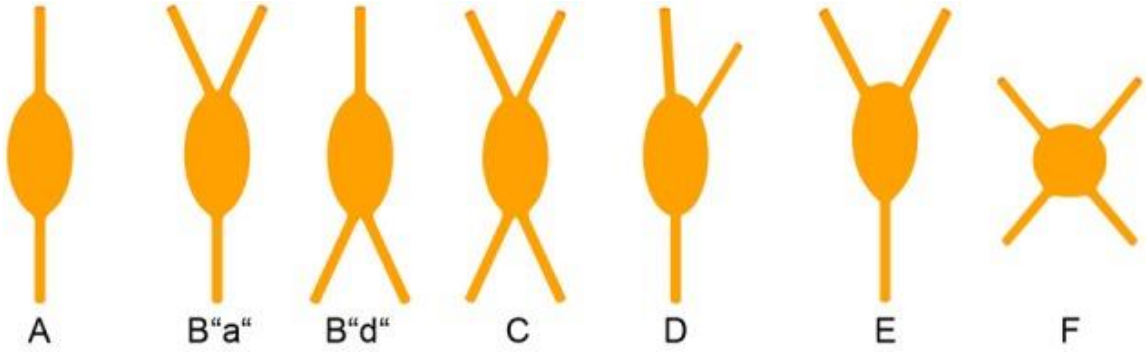

Figure 3. Calretinin (CR) interneuron morphology classification Cauli et al., 2014 classified CR cell shapes by dendritic patterns from the soma. (A) Bipolar: Two dendrites sprout from opposite side of soma. (B) Single Tufted: At least 2 dendrites originate from the opposite side of single dendrite (C) Bitufted: Two dendritic tufts originate from opposite sides of soma. (D) Modified: Among (A), (B), (C) which possesses a third dendrite that sprouts from the origin that is not identified above. (E) Tripolar: When this term is used, refer them back to either D or F, since it is difficult to classify. (F) Multipolar: At least 4(or 3) dendrite originates from soma. Figure and descriptions are from the Cauli et al., 2014.

\

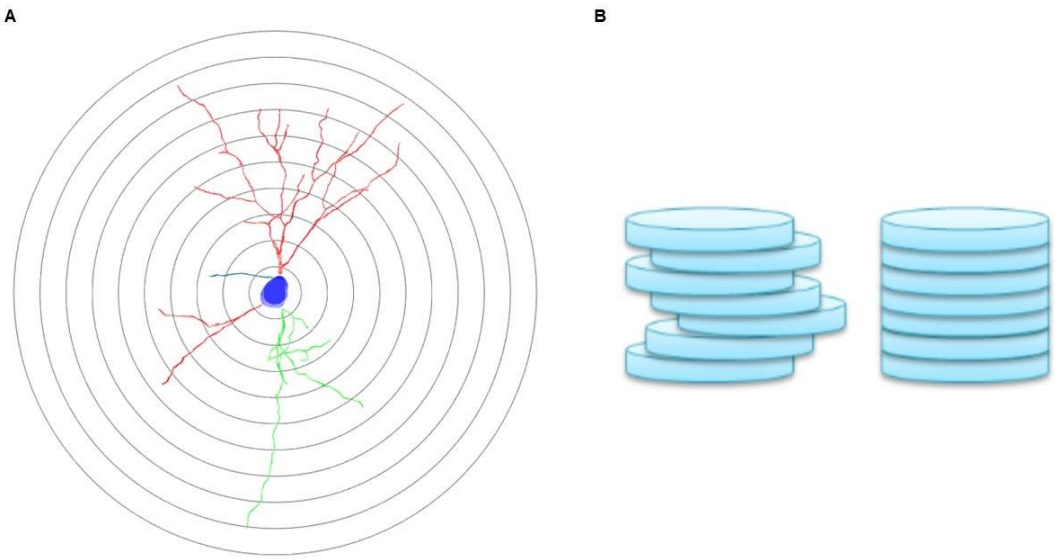

Figure 4. Demonstration of main analytical methods A, Graphical representation of Sholl analysis, black lines are 10μm spaced 3D sphere shells. Shells are centered at the centroid of the cell (blue). Red, green, light blue colored lines depict dendrites. B, Surface area and volume measure principle used by Neurolucida 360 Explorer (MBF Bioscience). Two stacks of discs have same surface area and volume. Images are imported from Neurolucida explorer user guide (v.2019.2.1)

RESULTS

3D Interneuron Morphological Properties

All neurons used for analysis were traced using NeuroLucida 360 (version 2019.1.1) with confocal image stacks acquired in 40x magnification (Fig 5B, D, F, H). Cells with an intact soma were selected and traced (Fig 5A, C, E, G). One to ten cells per image stack were traced (Fig 5I). Dendrites were traced until they appeared to end, indicated by no further IHC staining. Finished tracings went through automated analysis via NeuroLucida 360 explorer. Analyzed results of tracings are organized in Table 1.

First, soma to pia distance for neurons in each brain region was compared. Mean measured distances were, 325.1 ± 23 (Mky V1), 262.8 ± 16 (Mse V1), 363 ± 21 (Mky LPFC), 265.8 ± 25 (Mse FC). Soma to pia distance of Monkey LPFC was significantly greater than that of mouse FC (Table 1, One-way ANOVA, Tukey, $P<0.05$). However, percent distance, which is acquired by the formula "CR marker to pia/White matter to pia" showed different results than soma to pia distance. Percent distance of monkey LPFC was significantly greater than that of monkey V1 ($P<0.05$) and mouse V1 was significantly greater than monkey V1 ($P<0.001$) interneurons (Table 1). All CR positive interneurons fall into a determination range of layer2/3 in all brain regions (see Materials and methods).

The total mean dendritic length of neurons in each brain region was measured and compared. Mouse V1 was the longest (337.5 ± 32μm) among all brain regions. The length was shortest in an order of monkey LPFC (180.3 ± 22μm), monkey V1 (190.5 ± 32μm), mouse FC (241.4 ± 28μm). CR interneuron dendrites in Mouse V1 were significantly

longer than that of monkey V1 ($P<0.01$). Inter-species differences were more dramatic than differences between brain regions.

The mean volume of the soma was largest in an order of monkey LPFC, mouse V1, mouse FC, and monkey V1. Soma volume ranged around $550\mu m^3$, except monkey V1, which was $410 \pm 22\mu m^3$. Surface area of soma ranked monkey V1, mouse FC, monkey LPFC and mouse V1 from largest to smallest (Table 1). Similar to the pattern of soma volume, the surface area of somas ranged similarly at $300\mu m^2$ except mouse V1, which was $251.8 \pm 7.7\mu m^2$. Mouse FC somas were significantly greater in soma volume and surface area than those of mouse V1 ($P<0.05$).

The number of nodes was ordered in the following decreasing order: mouse V1, mouse FC, monkey LPFC, and monkey V1. Mouse V1 had significantly greater node counts compared to mouse FC ($P<0.01$).

Table 1. Morphological properties of CR interneuron Table of measurements of total length, soma volume, soma surface area, number of nodes, soma to pia distance, and percentage among reconstructed interneurons in monkey V1, monkey LPFC, mouse V1, and mouse FC. One-way anova and Tukey post-hoc analysis were used. Standard error of mean was used to depict data range.

	MkyV1	MkyLPFC	MseV1	MseFC	Mky versus mky LPFC versus V1	Mse versus mse FC versus V1	Mky versus mse LPFC versus FC	Mky versus mse V1 versus V1
Total length (µm)	190.5 ± 32	180.3 ± 22	337.5 ± 32	241.4 ± 28	ns	ns	ns	P<0.01
Soma volume (µm^3)	410 ± 22	556.7 ± 46	549.2 ± 55	545 ± 34	ns	P<0.05	ns	ns
Somal SA (µm^2)	305.1 ± 23	294.0 ± 15	251.8 ± 7.7	304.4 ± 12	ns	P<0.05	ns	ns
Nodes	2.4 ± 0.49	1.9 ± 0.25	3.8 ± 0.49	2.2 ± 0.29	ns	P<0.01	ns	ns
Soma to pia distance (µm)	325.1 ± 23	363 ± 21	262.8 ± 16	265.8 ± 25	ns	ns	P<0.05	ns
Percent distance from pia (%)	17.5 ± 1.1	20.8 ± 1.4	29.1 ± 1.8	22.82 ± 2.2	P<0.05	ns	ns	P<0.001

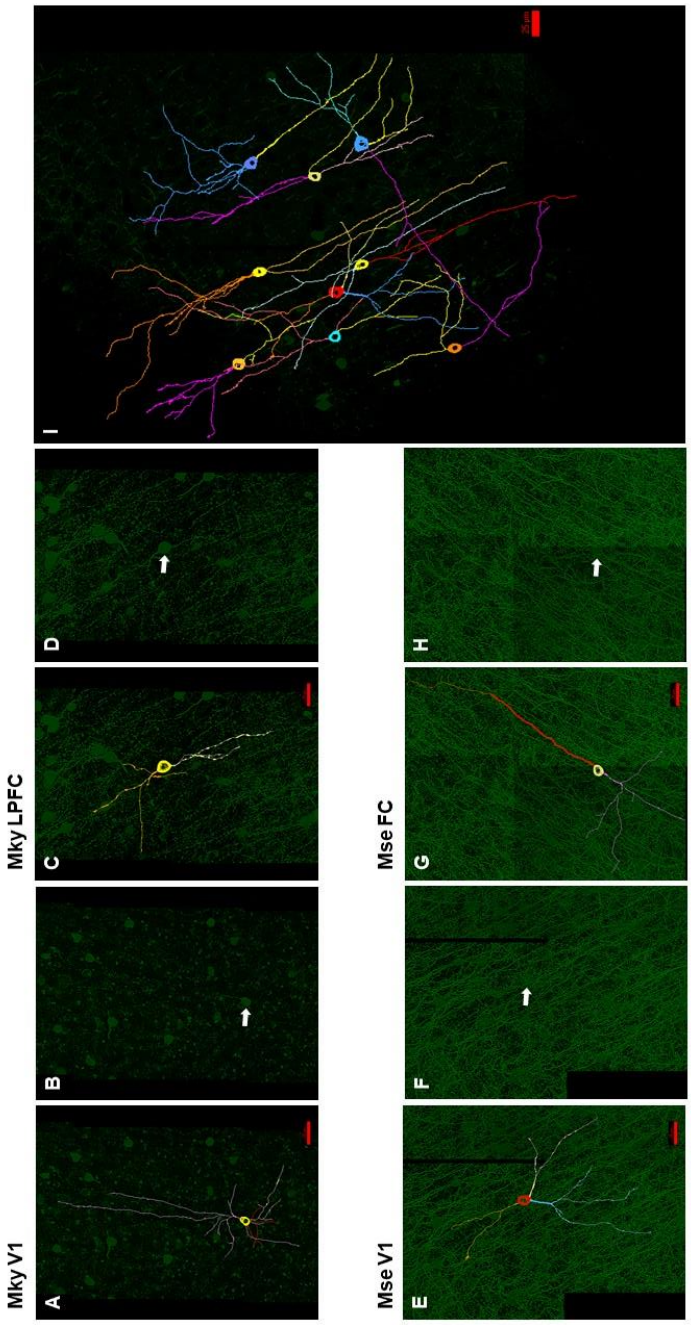

Figure 5. 3D reconstruction examples on deconvoluted image stacks. A, an example of interneuron reconstruction in monkey V1. B, max projection of deconvoluted image stacks of monkey V1, C, an example of interneuron reconstruction in monkey LPFC. D, max projection of deconvoluted image stacks of monkey LPFC, E, an example of interneuron reconstruction in mouse V1. F, max projection of deconvoluted image stacks of mouse V1, G, an example of interneuron reconstruction in mouse LPFC. H, max projection of deconvoluted image stacks of mouse LPFC, I, an example of fully reconstructed image stacks. All scale bars are 25μm long. Cell bodies in reconstructed interneurons are highlighted with the white arrow in deconvoluted image stacks.

Morphological Type Distribution of CR Interneurons

Calretinin interneuron populations of mouse and monkey brain regions were classified by a previous classification method (Cauli et al, 2014, Fig 2). Interneurons with one dendrite originating from soma's extreme were sorted as bipolar (Fig 6A, E). The angle between dendritic origin at the extreme and extra dendritic origin in close proximity was used to distinguish between single tufted and modified neurons. Neurons with an extra dendrite origin located less than 45 degrees from normal bipolar dendrite position were sorted as single tufted type (Fig 6B, F). Other neurons with extra dendrite origin farther than 45 degrees were sorted as modified (Fig 6C, H). Neurons with more than 4 dendritic origins which were 45 degrees apart from each other are classified as multipolar types (Fig 6D, I). The bitufted type was only found in mouse FC (Fig 6G, 7D) and this morphological type had two dendritic origins with 45-degree proximity on each extreme of soma.

Mouse CR+ interneurons tended to have relatively longer dendrites compared to their soma size, while monkey ones tended to have shorter dendrites. Unlike pyramidal-shaped soma of pyramidal neurons, interneurons somas generally had circular to oval shapes (Fig 6A-I).

All reconstructed cells were manually identified and assigned to previously described types. Figure 7 shows the results of the manual identification of each cell in the respective brain regions. Bipolar types comprise the majority of CR cell populations in monkey LPFC (Fig 7A, 64%, 14 cells) and both brain regions of the mouse (Fig 7C, D, 62% for Mse V1, 16 cells and 43% for Mse FC, 12 cells). The modified type was the most common cell type in Monkey V1 (Fig 7B, 39%, 7 cells), while in other regions it only

consisted as third most prevalent cell type (Fig 7A, C, D, 9% for Mky LPFC, 2 cells, 11% for Mse V1, 3 cells and 14% for Mse FC, 4 cells). The single tufted type was the second most popular cell type in monkey LPFC (Fig 7A, 27%, 6 cells) and both mouse brain regions (Fig 7C, D, 23% for Mse V1, 6 cells, and 21% for Mse FC, 6 cells), while it reached the fourth most popular cell type in Mky V1 (Fig 7B, 16%, 3 cells). Due to the limited sample population, there was only one bitufted neuron, which was found in mouse FC, thus comprising 4% of the total population of the brain region. (Fig 7A-D).

Overall monkey V1 showed distinctive population distribution, however, there were V1 and frontal regions followed a similar, but a slightly less exaggerated pattern.

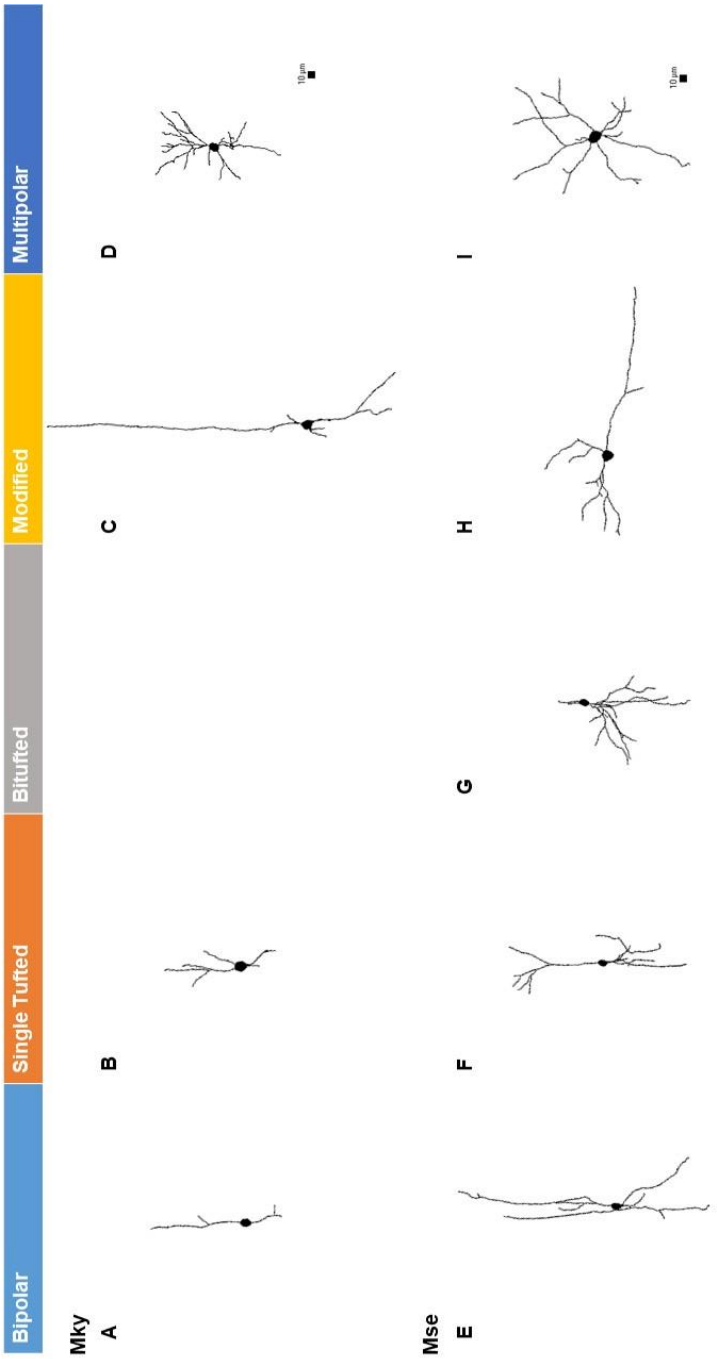

Figure 6. Morphological representations of calretinin cell types in monkey brain and mouse brain regions. A, Monkey bipolar Neuron, B, Monkey single tufted Neuron, C, Monkey modified neuron, D, Monkey multipolar Neuron, E, Mouse Bipolar Neuron, F, Mouse single tufted neuron, G, Mouse bitufted neuron, H, Mouse modified neuron, I, Mouse multipolar neuron. All cells are oriented in a way of pial surface to up and white matter to bottom. Color codes match with the ones of pie chart. Scale bar sizes are 10μm.

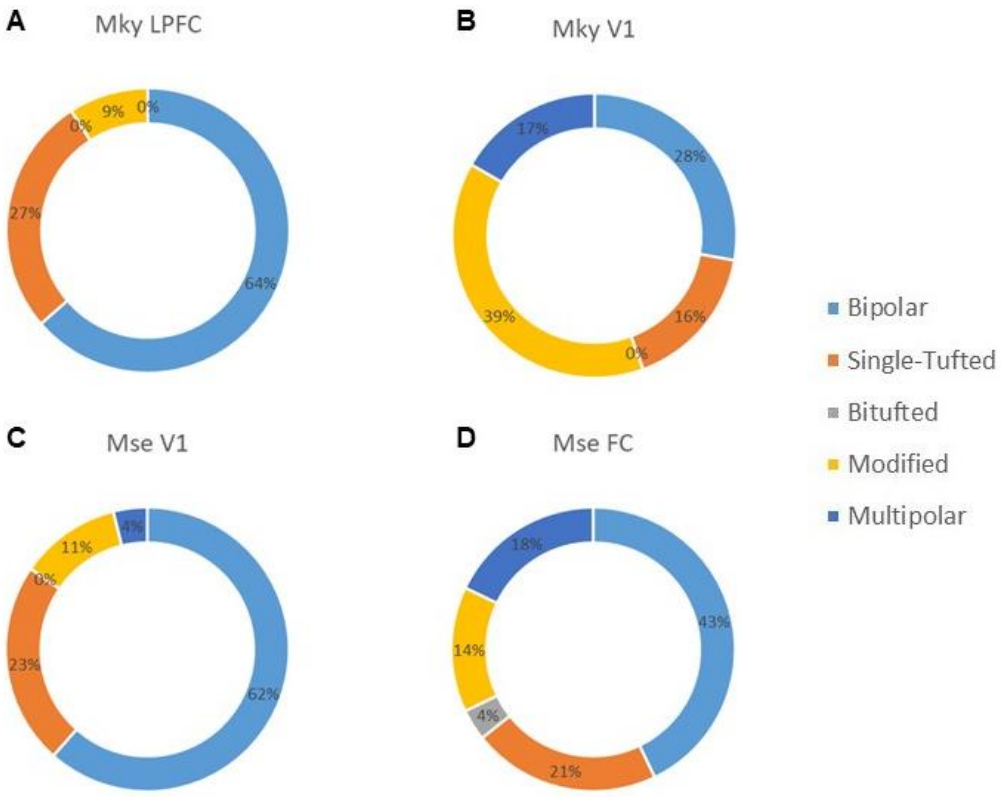

Figure 7. Proportions of calretinin interneuron cell types in mouse FC, V1 and monkey LPFC, V1. A, CR interneuron population distribution of Monkey LPFC, B, CR interneuron population distribution of Monkey V1, C, CR interneuron population distribution of Mouse V1, D, CR interneuron population distribution of Mouse FC. Cell types are color coded and depicted in legend on side. Bipolar as light blue, single tufted as orange, bitufted as gray, modified as yellow, and multipolar as navy.

CR Interneuron Morphology; Sholl Analysis

Sholl analysis was performed with 10μm spaced radii to acquire somatofugal morphology data of 3D reconstructed CR interneurons in monkey LPFC, monkey V1, mouse FC, and mouse V1. The interaction with radius shells provided data on the number of intersections, total length of all processes passing through, surface area, and average diameter.

The first parameter, intersections, showed a significant difference between groups (Fig 8A, One-way ANOVA, $P<0.005$). The Bonferonni post-hoc analysis revealed that CR cells in mouse FC have significantly higher intersection count compared to that of monkey PFC (Fig 8C, $P<0.0001$). However, no other between or within species difference was observed (Table 2, Fig 8B, D, E)

The second parameter, length, indicates mean length passing through the shell. There was a significant difference between groups found by one-way ANOVA (Fig 9A, $P<0.005$). Similar to the results of intersections, the Bonferroni post-hoc test showed a significant difference between monkey PFC and mouse FC (Fig 9C, $P<0.0001$). Mouse processes were longer than monkey ones at all radii measuring points. No other between-group analyses were found significant (Table 2, Fig 9B, D, E).

The third parameter, surface area, measured the intersecting surface area of the dendritic tree with the shell. By performing a one-way ANOVA analysis, the main effect was shown between groups (Fig 10A, $P<0.0001$). Also, there was a significant difference between monkey V1 versus mouse V1 (Bonferroni, $P<0.05$). Monkey V1 had a larger surface area crossing until the 40μm radius and mouse V1 had a larger surface on sections

after 50μm (Fig 10B). Also, monkey PFC and mouse FC showed similar patterns with previously described parameters. Mouse FC had a significantly larger surface area than monkey LPFC (Fig 10C, $P<0.0001$). Other regions did not show a significant effect in post-hoc analysis (Table 2, Fig 10D, E)

The last parameter, average diameter showed different graphic representations than the other three parameters (Fig 11A). However, the main effect of one-way ANOVA was significant ($P<0.0001$) like other parameters. Bonferroni post-hoc test revealed significant differences between monkey V1 versus mouse V1 (Fig 11B, $P<0.005$) and monkey PFC versus mouse FC (Fig 11C, $P<0.05$). Additionally, within species difference of monkey was first observed (Fig 11D, $P<0.0005$). No within species difference of mouse was found (Table 2, Fig 11E).

Table 2. Sholl analysis result comparison within species and brain regions. Rows represent mesurement of interest in sholl analysis; Intersections, length, surface area, and average diameter. One way anova was used for analysis. Bonferroni post-hoc test was used.

	Mky versus mky LPFC versus V1	Mse versus mse FC versus V1	Mky versus mse LPFC versus FC	Mky versus mse V1 versus V1
Intersections	ns	ns	P<0.0001	ns
Length (μm)	ns	ns	P<0.0001	ns
Surface area (μm^2)	ns	ns	P<0.0001	P<0.05
Average Diameter (μm)	P<0.0005	ns	P<0.05	P<0.005

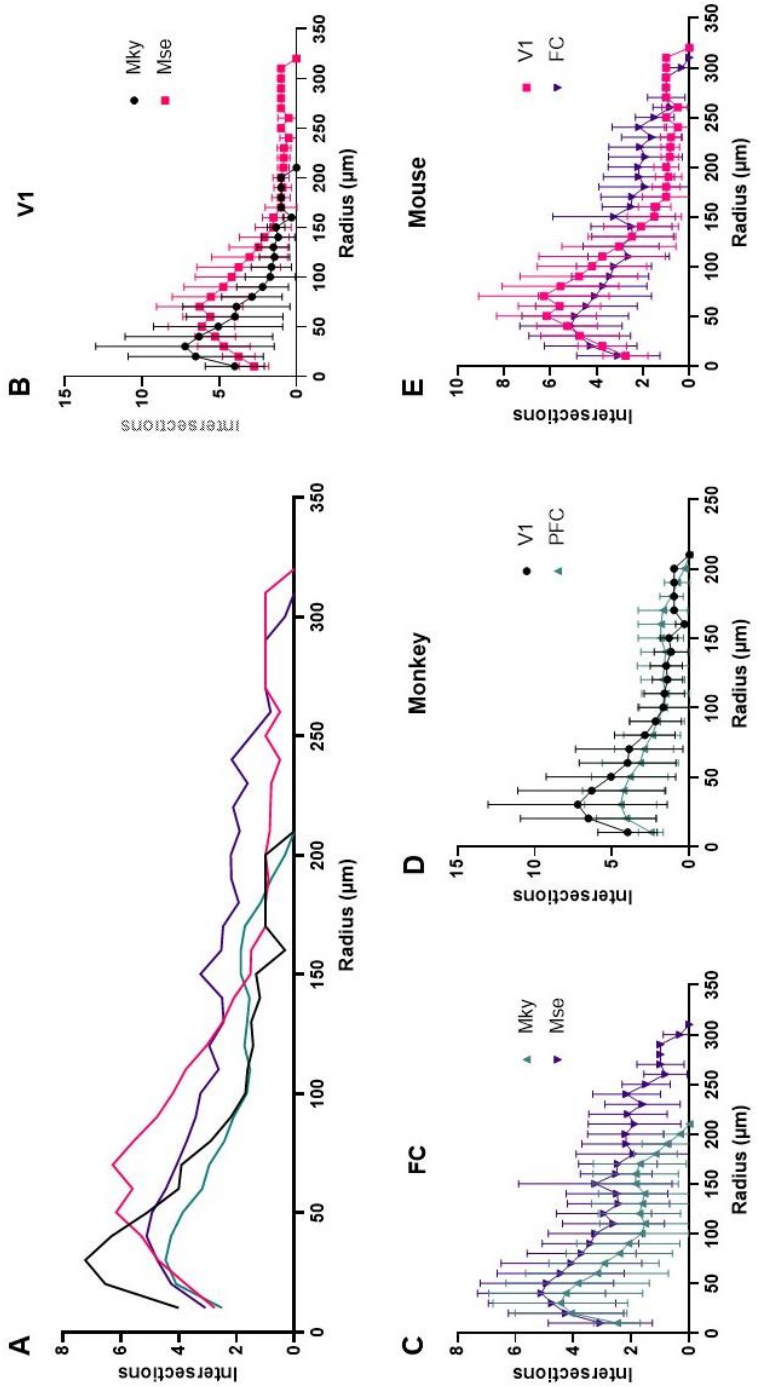

Figure 8. Interaction Sholl analysis. A, Distribution of mean number of intersections with 10µm increase. Monkey V1, LPFC, and mouse V1, FC is depicted on the graph. Color code is consistent with following charts. Starting point of all graphs are 10µm. B, Comparison of Monkey V1 versus Mouse V1. C, Comparison of Monkey LPFC versus mouse FC. D, Comparison of monkey LPFC versus monkey V1. E, Comparison of mouse FC versus mouse V1.

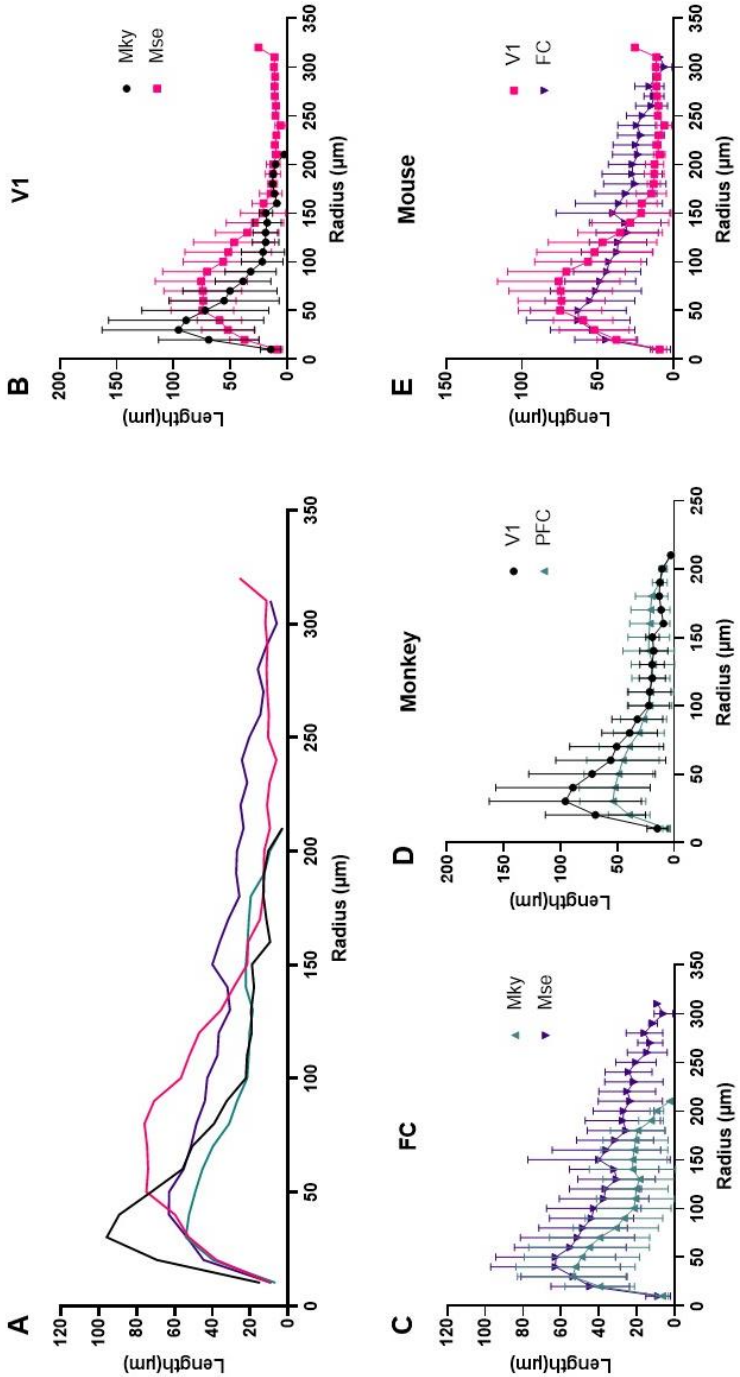

Figure 9. Length Sholl analysis. A, Distribution of mean length passing through the shell with 10μm increase, B, Comparison of Monkey V1 and Mouse V1, C, Comparison of Monkey LPFC and mouse FC, D, Within species comparison of monkey V1 versus LPFC, E, Within species comparison of mouse V1 versus FC.

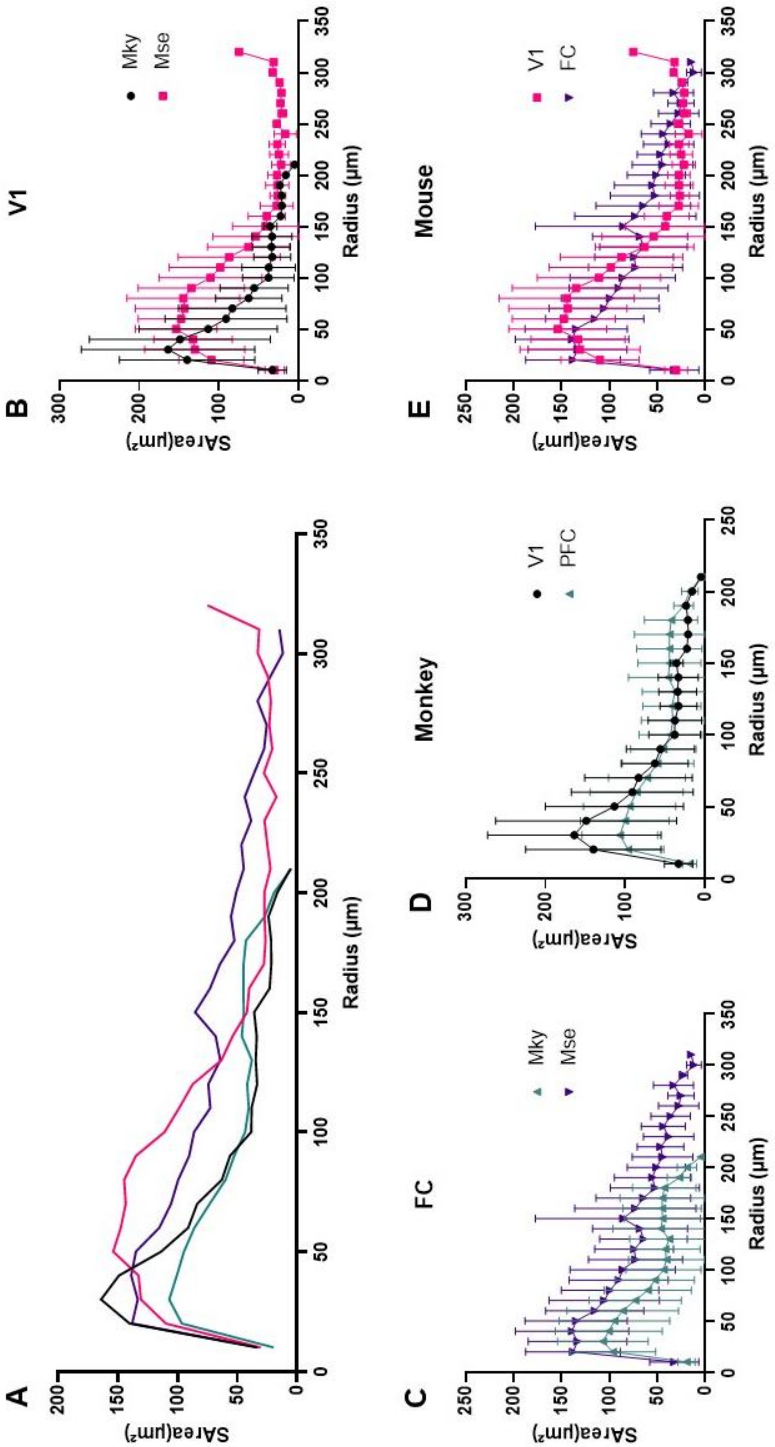

Figure 10. Surface area Sholl analysis. A, Distribution of surface areas of dendritic intersection with 10µm spaced shells, B, Comparison of Monkey V1 and Mouse V1, C, Comparison of Monkey LPFC and mouse FC, D, Within species comparison of monkey V1 versus LPFC, E, Within species comparison of mouse V1 versus FC.

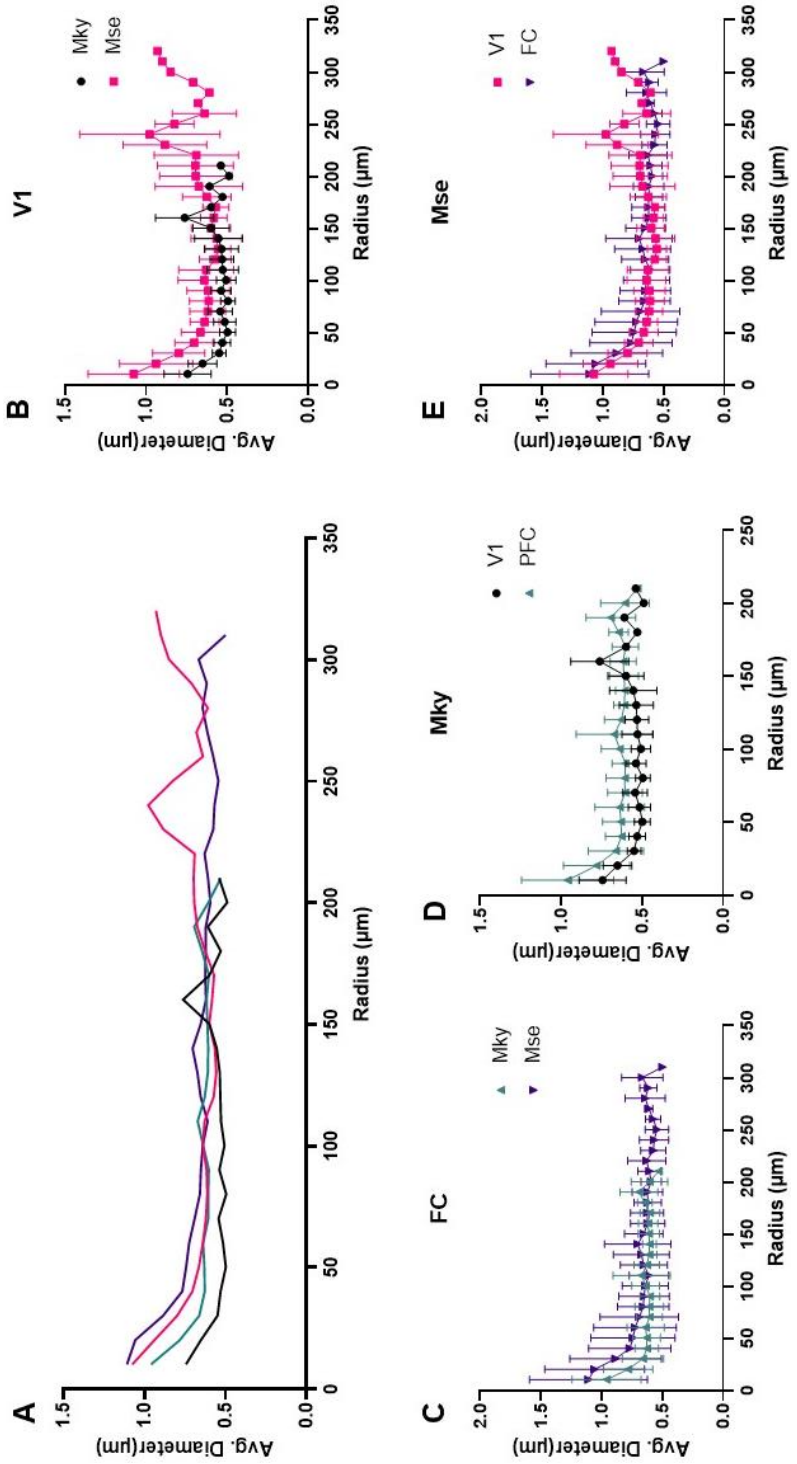

Figure 11. Average diameter Sholl analysis. A, Distribution of average diameter of dendrites crossing a shell with 10µm increase, B, Comparison of Monkey V1 and Mouse V1, C, Comparison of Monkey LPFC and mouse FC, D, Within species comparison of monkey V1 versus LPFC, E, Within species comparison of mouse V1 versus FC.

DISCUSSION

One of the major challenges of modern neuroscience research is to understand the cellular characteristics of cortical circuits. In our lab, multiple studies about the pyramidal neurons, one of the building blocks of neural circuits, have been performed (Chang et al, 2005, Luebke et al, 2015, Gilman et al, 2017). However, comparative characteristics of interneurons, the other key participants of neural circuits, are relatively poorly understood. The purpose of this study was to address the question of whether and how specific monkey and mouse interneuron populations may differ. Based on a previous comparative study between mouse and monkey (Gilman et al, 2017), we hypothesized that differences between interneurons in different brain areas and between species do exist. Therefore, we conducted a comparative study between mouse and rhesus monkey calretinin (CR) and parvalbumin (PV) positive interneuron populations.

However, immunohistochemistry results of PV on monkey and mouse tissue showed no dendritic branching or flimsy processes, which were not prominent enough to perform the 3D reconstruction. Among PV and CR interneurons, only CR+ interneurons were able to be morphologically compared. We aimed to work on interneuron populations in layer 2 and layer 3 in order to be consistent with the previous comparative study on pyramidal neurons in these layers and therefore to and connect the interneuron data with pyramidal neuron data.

According to the differences of dendritic length and node counts between Mouse V1 and Monkey V1, we have shown that mouse CR+ interneuron dendrites have longer

and more complex dendritic arbors compared to those in the monkey. This result coincides with the morphological differences of pyramidal neurons in respective brain areas in each species, which was already revealed in the previous comparative study (Gilman et al, 2017). In pyramidal neuron study, monkey V1 showed shorter length in both apical and basal dendrites compared to mouse V1. We first assumed that CR+ interneurons follow size ratios of pyramidal neurons in respective brain areas, which matches with V1 interneuron size differences. But this theory does not explain inter-species CR+ interneuron size difference of frontal cortices. Thus, we think the size relationship only applies to CR+ interneurons in V1s, which could indicate a relationship with pyramidal neurons.

More dendritic nodes in mouse V1 CR+ interneuron populations could presumably mean more connections, which mainly synapse on other GABAergic interneurons for disinhibition (Cauli et al, 2014). A joint study with this project, done by Rakin Nasar, came up with a result showing significantly more Vgat+ bouton co-localization with PV+ boutons. This result indicates either more GABAergic interneuron counts on mouse V1 or stronger disinhibition effect on PV+ interneuron from outer sources. Previous pyramidal neuron comparative study of monkey V1 showed lower spine counts on V1 dendrites compared to mouse ones (Gilman et al, 2017). We can assume a number of inhibitory synaptic connection is also lower based on that lower spine counts. Which possibly indicate lower dendritic arborization of other GABAergic neurons or fewer number of its population.

We moved on to the cell type analysis of the reconstructed cell population. We first followed the guidelines of previous sorting criteria made by Cauli et al (2014). However,

we soon found that the distinctions between single tufted types and modified types in our sample group were not straightforward. Often times, dendritic origins were placed slightly farther than 20 degrees from each other, but no dendrites were clearly positioned at extreme of soma, so it was difficult to apply the previous sorting method. So we derived a new method using instead of 20 degrees from the upper or lower pole of soma, we increased the limit to 40 degrees for the sorting rule between single tufted and modified types.

As shown in figure 7, cellular distribution remained similar across species and brain areas except for monkey V1. A low proportion of bipolar neurons (28%) was shown. Such result can be connected to specific targeting of the interneuron population. According to Džaja et al (2014), synaptic targets of CR+ cells can be identified by their morphological types. A few numbers of bipolar proportion in monkey V1 could indicate less connection between CR+ interneurons and the apical dendrite of pyramidal cells. The author also suggested another type of CR+ cells, double-bouquet cells, connect primarily to the basal dendrite of pyramidal cells, which could be the main synaptic formation of monkey V1 in this study. However, classification guidelines for double bouquet cells are unclear, which may not be applicable for pre-determined cell types of this study.

The orientation of cells was determined by two major dendritic branches originating from the soma. Most dendrites were perpendicular to the pia, except for in multipolar cells that have multidirectional dendritic branching. However, there was one exception of a modified neuron (Fig 6H) in which the direction of dendrites was parallel to the pia. This cell was found close to the pia and several other similar-looking cells were observed during counting analysis, which was a part of the joint project with this one. Due to its peculiar

location and morphology, CR+ interneurons with these morphological features may have a different role than members of other populations. There is a low chance of them connecting to PV+ interneurons because a majority of PV interneurons are concentrated at layer 4-6. Those horizontal CR interneurons may have other GABAergic interneuron targets that are close to pia, or it could be connecting between CR interneurons for activity modulation.

The results from Sholl analysis showed several inter-species differences between CR+ interneurons in mouse FC versus monkey LPFC. In general, mouse interneurons had smaller soma but were larger in overall size than monkey ones. In the pyramidal neuron study, the LPFC neurons were larger than mouse PFC ones, but monkey V1 neurons were smaller than mouse V1 ones. So, we can tell the size principle of CR+ cells in relation to pyramidal cell size ratio is only applicable for the V1 region, which agrees with the previous results from the dendritic length and node analysis.

Sholl analysis revealed a sudden increase in the average diameter of dendrites in V1 neurons of both species. The peak of the increase occurred at the 160μm from soma for monkey cells out of 210μm total distance, and mouse one had its peak at 240μm out of 320μm total distance from the soma. In a percentage-wise, monkey and mouse peak occurred at similar points (mky 76.2%, mse 75%). We suspect this phenomenon is not random. Rather, this could be the indication of V1 region-specific CR+ cell morphological properties. In the 3D morphological analysis, CR+ neurons in V1 of both species also exhibit more node counts than FC regions. Taken together, these results could be

interpreted as V1 CR+ interneurons tend to branch out more in dendrites after 75% of its length progression and node counts in each Sholl shell would further support this claim.

This study demonstrated the morphological characteristics of CR+ interneurons and how do they differ by species and brain areas. The results have shown distinct features of monkey and mouse V1. Both monkey and mouse V1 have shown more dendritic arborization than monkey LPFC and mouse PFC. A comparison between monkey and mouse V1 showed lower inhibitory synapse numbers on pyramidal neurons from other GABAergic interneurons on Monkey V1. Also, the peculiar cell type distribution of monkey V1 may indicate different synaptic target preferences of CR+ interneurons. Although the study met limitations due to the lack of PV+ cell data, we have made some useful remarks of CR+ cells. CR+ interneurons are considered to play an important role in higher-order brain functions, which could be related to the evolution of cognitive functioning (Džaja et al, 2014). We expect more studies regarding CR+ interneurons will emerge and hope our work serves as a stepping stone for future research.

BIBLIOGRAPHY

Arkhipov, A., Gouwens, N. W., Billeh, Y. N., Gratiy, S., Iyer, R., Wei, Z., et al. (2018); Visual physiology of the layer 4 cortical circuit in silico. *PLoS computational biology,* 14(11), e1006535.

Barinka, F., Druga, R. (2010); Calretinin expression in the mammalian neocortex: a review. *Physiological research,* 59(5), 665-677.

Barton, R. A. (1996); Neocortex size and behavioural ecology in primates. *Proceedings. Biological sciences,* 263(1367), 173-177.

Bartos, M., Vida, I., Jonas, P. (2007); Synaptic mechanisms of synchronized gamma oscillations in inhibitory interneuron networks. *Nature reviews. Neuroscience,* 8(1), 45-56.

Bicks, L. K., Yamamuro, K., Flanigan, M. E., Kim, J. M., Kato, D., Lucas, E. K., et al. (2020); Prefrontal parvalbumin interneurons require juvenile social experience to establish adult social behavior. *Nature communications,* 11(1), 1003.

Bogus-Nowakowska, K. (2019); Ontogeny of Neurons Containing Calcium-Binding Proteins in the Preoptic Area of the Guinea Pig: Sexually Dimorphic Development of Calbindin. *Developmental neurobiology,* 79(2), 175-201.

Camp, A. J., Wijesinghe, R. (2009); Calretinin: modulator of neuronal excitability. *The international journal of biochemistry & cell biology,* 41(11), 2118-2121.

Carlén, M. (2017); What constitutes the prefrontal cortex. *Science (New York, N.Y.),* 358(6362), 478-482.

Caroni, P. (2015); Regulation of Parvalbumin Basket cell plasticity in rule learning. *Biochemical and biophysical research communications,* 460(1), 100-103.

Cauli, B., Zhou, X., Tricoire, L., Toussay, X., Staiger, J. F. (2014); Revisiting enigmatic cortical calretinin-expressing interneurons. *Frontiers in neuroanatomy,* 8, 52.

Celio, M. R., Heizmann, C. W. (1982); Calcium-binding protein parvalbumin is associated with fast contracting muscle fibres. *Nature,* 297(5866), 504-506.

Chang, Y. M., Rosene, D. L., Killiany, R. J., Mangiamele, L. A., Luebke, J. I. (2005); Increased action potential firing rates of layer 2/3 pyramidal cells in the prefrontal cortex are significantly related to cognitive performance in aged monkeys. *Cerebral cortex (New York, N.Y. : 1991),* 15(4), 409-418.

Chen, J. Y., Wang, E. A., Cepeda, C., Levine, M. S. (2013); Dopamine imbalance in Huntington's disease: a mechanism for the lack of behavioral flexibility. *Frontiers in neuroscience*, 7, 114.

Connor, C. E. (2000); Visual perception: monkeys see things our way. *Current biology : CB*, 10(22), R836-8.

Dawson, T. M., Golde, T. E., Lagier-Tourenne, C. (2018); Animal models of neurodegenerative diseases. *Nature neuroscience*, 21(10), 1370-1379.

DeFelipe, J., López-Cruz, P. L., Benavides-Piccione, R., Bielza, C., Larrañaga, P., Anderson, S., et al. (2013); New insights into the classification and nomenclature of cortical GABAergic interneurons. *Nature reviews. Neuroscience*, 14(3), 202-216.

Džaja, D., Hladnik, A., Bičanić, I., Baković, M., Petanjek, Z. (2014); Neocortical calretinin neurons in primates: increase in proportion and microcircuitry structure. *Frontiers in neuroanatomy*, 8, 103.

Descalzo, V. F., Nowak, L. G., Brumberg, J. C., McCormick, D. A., Sanchez-Vives, M. V. (2005); Slow adaptation in fast-spiking neurons of visual cortex. *Journal of neurophysiology*, 93(2), 1111-1118.

Dudchenko, P. A. (2004); An overview of the tasks used to test working memory in rodents. *Neuroscience and biobehavioral reviews*, 28(7), 699-709.

Faas, G. C., Schwaller, B., Vergara, J. L., Mody, I. (2007); Resolving the fast kinetics of cooperative binding: Ca2+ buffering by calretinin. *PLoS biology*, 5(11), e311.

Fairén, A., Lorente, R. d. e. . N. (2007); Cajal and Lorente de Nó on cortical interneurons: coincidences and progress. *Brain research reviews*, 55(2), 430-444.

Ferguson, B. R., Gao, W. J. (2018); PV Interneurons: Critical Regulators of E/I Balance for Prefrontal Cortex-Dependent Behavior and Psychiatric Disorders. *Frontiers in neural circuits*, 12, 37.

Fogarty, M., Grist, M., Gelman, D., Marín, O., Pachnis, V., Kessaris, N. (2007); Spatial genetic patterning of the embryonic neuroepithelium generates GABAergic interneuron diversity in the adult cortex. *The Journal of neuroscience : the official journal of the Society for Neuroscience*, 27(41), 10935-10946.

Fröhlich, F. (2016); Synaptic Plasticity in *Network Neuroscience*, 47-58

Fuster, J. M. (2001); The prefrontal cortex--an update: time is of the essence. *Neuron*, 30(2), 319-333.

Gelman, D. M., Martini, F. J., Nóbrega-Pereira, S., Pierani, A., Kessaris, N., Marín, O. (2009); The embryonic preoptic area is a novel source of cortical GABAergic interneurons. *The Journal of neuroscience : the official journal of the Society for Neuroscience,* 29(29), 9380-9389.

Ghosh, A., Rothwell, J., Haggard, P. (2014); Using voluntary motor commands to inhibit involuntary arm movements. *Proceedings. Biological sciences,* 281(1794), 20141139.

Gilman, J. P., Medalla, M., Luebke, J. I. (2017); Area-Specific Features of Pyramidal Neurons-a Comparative Study in Mouse and Rhesus Monkey. *Cerebral cortex (New York, N.Y. : 1991),* 27(3), 2078-2094.

Gonzalez-Burgos, G., Cho, R. Y., Lewis, D. A. (2015); Alterations in cortical network oscillations and parvalbumin neurons in schizophrenia. *Biological psychiatry,* 77(12), 1031-1040.

Götz, M., Huttner, W. B. (2005); The cell biology of neurogenesis. *Nature reviews. Molecular cell biology,* 6(10), 777-788.

Groves, P., Palczewska, M. (2001); Cation binding properties of calretinin, an EF-hand calcium-binding protein. *Acta biochimica Polonica,* 48(1), 113-119.

Gulyás, A. I., Megías, M., Emri, Z., Freund, T. F. (1999); Total number and ratio of excitatory and inhibitory synapses converging onto single interneurons of different types in the CA1 area of the rat hippocampus. *The Journal of neuroscience : the official journal of the Society for Neuroscience,* 19(22), 10082-10097.

Hara, Y., Rapp, P. R., Morrison, J. H. (2012); Neuronal and morphological bases of cognitive decline in aged rhesus monkeys. *Age (Dordrecht, Netherlands),* 34(5), 1051-1073.

Hu, H., Gan, J., Jonas, P. (2014); Interneurons. Fast-spiking, parvalbumin^{+} GABAergic interneurons: from cellular design to microcircuit function. *Science (New York, N.Y.),* 345(6196), 1255263.

Huang, Z. J., Di Cristo, G., Ango, F. (2007); Development of GABA innervation in the cerebral and cerebellar cortices. *Nature reviews. Neuroscience,* 8(9), 673-686.

Hubel, D. H., Wiesel, T. N. (1962); Receptive fields, binocular interaction and functional architecture in the cat's visual cortex. *The Journal of physiology,* 160, 106-154.

Justice, M. J., Dhillon, P. (2016); Using the mouse to model human disease: increasing validity and reproducibility. *Disease models & mechanisms,* 9(2), 101-103.

Kawaguchi, Y., Kubota, Y. (1997); GABAergic cell subtypes and their synaptic connections in rat frontal cortex. *Cerebral cortex (New York, N.Y. : 1991),* 7(6), 476-486.

Kim, D., Jeong, H., Lee, J., Ghim, J. W., Her, E. S., Lee, S. H., Jung, M. W. (2016); Distinct Roles of Parvalbumin- and Somatostatin-Expressing Interneurons in Working Memory. *Neuron,* 92(4), 902-915.

Klausberger, T., Somogyi, P. (2008); Neuronal diversity and temporal dynamics: the unity of hippocampal circuit operations. *Science (New York, N.Y.),* 321(5885), 53-57.

Koestinger, G., Martin, K. A. C., Rusch, E. S. (2018); Translaminar circuits formed by the pyramidal cells in the superficial layers of cat visual cortex. *Brain structure & function,* 223(4), 1811-1828.

Konecky, R. O., Smith, M. A., Olson, C. R. (2017); Monkey prefrontal neurons during Sternberg task performance: full contents of working memory or most recent item. *Journal of neurophysiology,* 117(6), 2269-2281.

Lim, L., Mi, D., Llorca, A., Marín, O. (2018); Development and Functional Diversification of Cortical Interneurons. *Neuron,* 100(2), 294-313.

Lindenfors, P. (2005); Neocortex evolution in primates: the "social brain" is for females. *Biology letters,* 1(4), 407-410.

Luebke, J. I., Medalla, M., Amatrudo, J. M., Weaver, C. M., Crimins, J. L., Hunt, B., et al. (2015); Age-related changes to layer 3 pyramidal cells in the rhesus monkey visual cortex. *Cerebral cortex (New York, N.Y. : 1991),* 25(6), 1454-1468.

Marín, O. (2012); Interneuron dysfunction in psychiatric disorders. *Nature reviews. Neuroscience,* 13(2), 107-120.

Mattson, M. P., Kater, S. B. (1987); Calcium regulation of neurite elongation and growth cone motility. *The Journal of neuroscience : the official journal of the Society for Neuroscience,* 7(12), 4034-4043.

Meganathan, K., Lewis, E. M. A., Gontarz, P., Liu, S., Stanley, E. G., Elefanty, A. G., Huettner, J. E., Zhang, B., Kroll, K. L. (2017); Regulatory networks specifying cortical interneurons from human embryonic stem cells reveal roles for CHD2 in interneuron development. *Proceedings of the National Academy of Sciences of the United States of America,* 114(52), E11180-E11189.

Nei, M., Glazko, G. V. (2002); The Wilhelmine E. Key 2001 Invitational Lecture. Estimation of divergence times for a few mammalian and several primate species. *The Journal of heredity,* 93(3), 157-164.

Nichols, J., Bjorklund, G. R., Newbern, J., Anderson, T. (2018); Parvalbumin fast-spiking interneurons are selectively altered by paediatric traumatic brain injury. *The Journal of physiology,* 596(7), 1277-1293.

Phillips, K. A., Bales, K. L., Capitanio, J. P., Conley, A., Czoty, P. W., 't Hart, B. A., et al. (2014); Why primate models matter. *American journal of primatology,* 76(9), 801-827.

Pouille, F., Scanziani, M. (2001); Enforcement of temporal fidelity in pyramidal cells by somatic feed-forward inhibition. *Science (New York, N.Y.),* 293(5532), 1159-1163.

Pouille, F., Marin-Burgin, A., Adesnik, H., Atallah, B. V., Scanziani, M. (2009); Input normalization by global feedforward inhibition expands cortical dynamic range. *Nature neuroscience,* 12(12), 1577-1585.

Priebe, N. J., McGee, A. W. (2014); Mouse vision as a gateway for understanding how experience shapes neural circuits. *Frontiers in neural circuits,* 8, 123.

Qi, G., Feldmeyer, D. (2016); Dendritic Target Region-Specific Formation of Synapses Between Excitatory Layer 4 Neurons and Layer 6 Pyramidal Cells. *Cerebral cortex (New York, N.Y. : 1991),* 26(4), 1569-1579.

Quiquempoix, M., Fayad, S. L., Boutourlinsky, K., Leresche, N., Lambert, R. C., Bessaih, T. (2018); Layer 2/3 Pyramidal Neurons Control the Gain of Cortical Output. *Cell reports*, 24(11), 2799-2807.e4.

Rakic, P. (2009); Evolution of the neocortex: a perspective from developmental biology. *Nature reviews. Neuroscience,* 10(10), 724-735.

Rogers, J. H. (1987); Calretinin: a gene for a novel calcium-binding protein expressed principally in neurons. *The Journal of cell biology,* 105(3), 1343-1353.

Schoenemann, P. T., Sheehan, M. J., Glotzer, L. D. (2005); Prefrontal white matter volume is disproportionately larger in humans than in other primates. *Nature neuroscience,* 8(2), 242-252.

Schwaller, B. (2014); Calretinin: from a "simple" Ca (2+) buffer to a multifunctional protein implicated in many biological processes. *Frontiers in neuroanatomy,* 8, 3.

Seamans, J. K., Lapish, C. C., Durstewitz, D. (2008); Comparing the prefrontal cortex of rats and primates: insights from electrophysiology. *Neurotoxicity research,* 14(2-3), 249-262.

Seok, J., Warren, H. S., Cuenca, A. G., Mindrinos, M. N., Baker, H. V., Xu, W., et al. (2013); Genomic responses in mouse models poorly mimic human inflammatory

diseases. *Proceedings of the National Academy of Sciences of the United States of America,* 110(9), 3507-3512.

Sun, T., Hevner, R. F. (2014); Growth and folding of the mammalian cerebral cortex: from molecules to malformations. *Nature reviews. Neuroscience*, 15(4), 217-232.

Sun, Q., Li, X., Li, A., Zhang, J., Ding, Z., Gong, H., et al. Ventral Hippocampal-Prefrontal Interaction Affects Social Behavior via Parvalbumin Positive Neurons in the Medial Prefrontal Cortex. *iScience,* 10.1016/j.isci.2020.100894

Teffer, K., Semendeferi, K. (2012); Human prefrontal cortex: evolution, development, and pathology. *Progress in brain research,* 195, 191-218.

Tremblay, R., Lee, S., Rudy, B. (2016); GABAergic Interneurons in the Neocortex: From Cellular Properties to Circuits. *Neuron,* 91(2), 260-292.

Uylings, H. B., Groenewegen, H. J., Kolb, B. (2003); Do rats have a prefrontal cortex. *Behavioural brain research,* 146(1-2), 3-17.

Vandamme, T. F. (2014); Use of rodents as models of human diseases. *Journal of pharmacy & bioallied sciences*, 6(1), 2-9.

Xu, X., Roby, K. D., Callaway, E. M. (2010); Immunochemical characterization of inhibitory mouse cortical neurons: three chemically distinct classes of inhibitory cells. *The Journal of comparative neurology*, 518(3), 389-404.

CURRICULUM VITAE